A Metal–Nitride Nanowire Dual–Photoelectrode Device for Unassisted Solar–to–Hydrogen Conversion under Parallel Illumination

5 AUTHORS, INCLUDING:

Bandar AlOtaibi
McGill University
14 PUBLICATIONS **65** CITATIONS

SEE PROFILE

Shimin Fan
Tsinghua University
55 PUBLICATIONS **278** CITATIONS

SEE PROFILE

Srinivas Vanka
McGill University
2 PUBLICATIONS **0** CITATIONS

SEE PROFILE

Md Golam Kibria
McGill University
**32** PUBLICATIONS **443** CITATIONS

SEE PROFILE

A Metal-Nitride Nanowire Dual-Photoelectrode Device for Unassisted Solar-to-Hydrogen Conversion under Parallel Illumination

B. AlOtaibi, S. Fan, S. Vanka, M. G. Kibria, and Z. Mi*

Department of Electrical and Computer Engineering, McGill University 3480 University Street, Montreal, Quebec H3A 0E9, Canada

Ⓢ Supporting Information

ABSTRACT: A dual-photoelectrode device, consisting of a photoanode and photocathode with complementary energy bandgaps, has long been perceived as an ideal scheme for achieving high efficiency, unassisted solar-driven water splitting. Previously reported 2-photon tandem devices, however, generally exhibit an extremely low efficiency (<0.1%), which has been largely limited by the incompatibility between the two photoelectrode materials. Here we show that the use of metal-nitride nanowire photoelectrodes, together with the scheme of parallel illumination by splitting the solar spectrum spatially and spectrally, can break the efficiency bottleneck of conventional 2-photon tandem devices. We have first investigated a dual-photoelectrode device consisting of a GaN nanowire photoanode and an InGaN nanowire photocathode, which exhibited an open circuit potential of 1.3 V and nearly 20-fold enhancement in the power conversion efficiency under visible light illumination (400−600 nm), compared to the individual photoelectrodes in 1 mol/L HBr. We have further demonstrated a dual-photoelectrode device consisting of parallel-connected metal-nitride nanowire photoanodes and a Si/InGaN nanowire photocathode, which can perform unassisted, direct solar-to-hydrogen conversion. A power conversion efficiency of 2% was measured under AM1.5G 1 sun illumination.
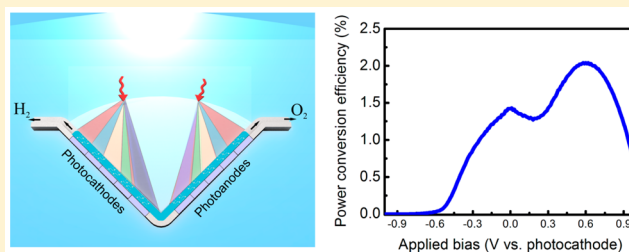
KEYWORDS: *Nanowire, InGaN, water splitting, hydrogen, solar fuels, dual-photoelectrode*

It has been envisioned that the artificial conversion of solar energy to clean fuels can potentially overcome the energy crisis in the future.[1] In this regard, photoelectrochemical (PEC) cells have been intensively studied, wherein solar energy can be directly converted into chemical fuels such as hydrogen.[2−4] Among the various PEC designs, a p/n dual-photoelectrode device, also commonly referred to as a photochemical diode, promises significant performance advantages and cost benefits.[5−12] First described by Nozik in 1977,[13,14] such a 2-photon dual-electrode system can be implemented with two semiconductors connected back-to-back in tandem, forming the top and bottom photoelectrode, which is an analogue of the Z-scheme in natural photosynthesis. In this scheme, minority carriers are driven to the semiconductor/liquid junction to perform oxidation/reduction reactions, while majority carriers recombine at the photocathode/anode interface. In a p/n dual-photoelectrode system, the electron−hole pair chemical potential can be made equal to, or greater than the largest band gap of the two semiconductors. As such, it can address the critical photovoltage bottleneck of a single-photoelectrode system, thereby leading to unassisted, solar-driven water splitting and H₂ generation.[15,16] Another fundamental advantage of the dual-photoelectrode system lies in that the two semiconductors can be designed to be complementary light absorbers. By separately optimizing the bandgap of the light absorption layers, the device efficiency can reach a theoretical maximum of 40% and 29.7% considering reasonable energy loss processes.[10,17] The p/n dual-photoelectrodes also offer several important advantages compared to photovoltaic-PEC (PV-PEC) and photovoltaic-electrolysis (PV-EL) technologies, including much simpler fabrication process, significantly reduced operation voltage, and potentially higher efficiency.[18−21] Beside the simple 2-photon p/n dual-photoelectrode, PV-PEC or PV-EL photoelectrodes can also be paired in a dual configuration to achieve improved solar-to-hydrogen efficiency.

Despite their promises, conventional 2-photon tandem photoelectrodes generally exhibit very poor performance with the commonly reported efficiency in the range of ∼0.1% or less,[11,22] which are significantly smaller than the best reported single photoelectrode (∼1.8%)[15,16] and PV-PEC devices (12.4%).[23] More recently, higher efficiency values (∼0.9%) have been demonstrated by using a hematite photoanode and amorphous Si photocathode with NiFeOₓ and TiO₂/Pt overlayers.[12] In previously reported tandem dual-photoelectrodes, dissimilar materials were used to provide complementary bandgaps. The resulting photovoltage is small, limited by the material quality and incompatibility.[11] Moreover, the device efficiency is severely compromised by the poor interfacial properties and in many cases by the performance of the Ohmic
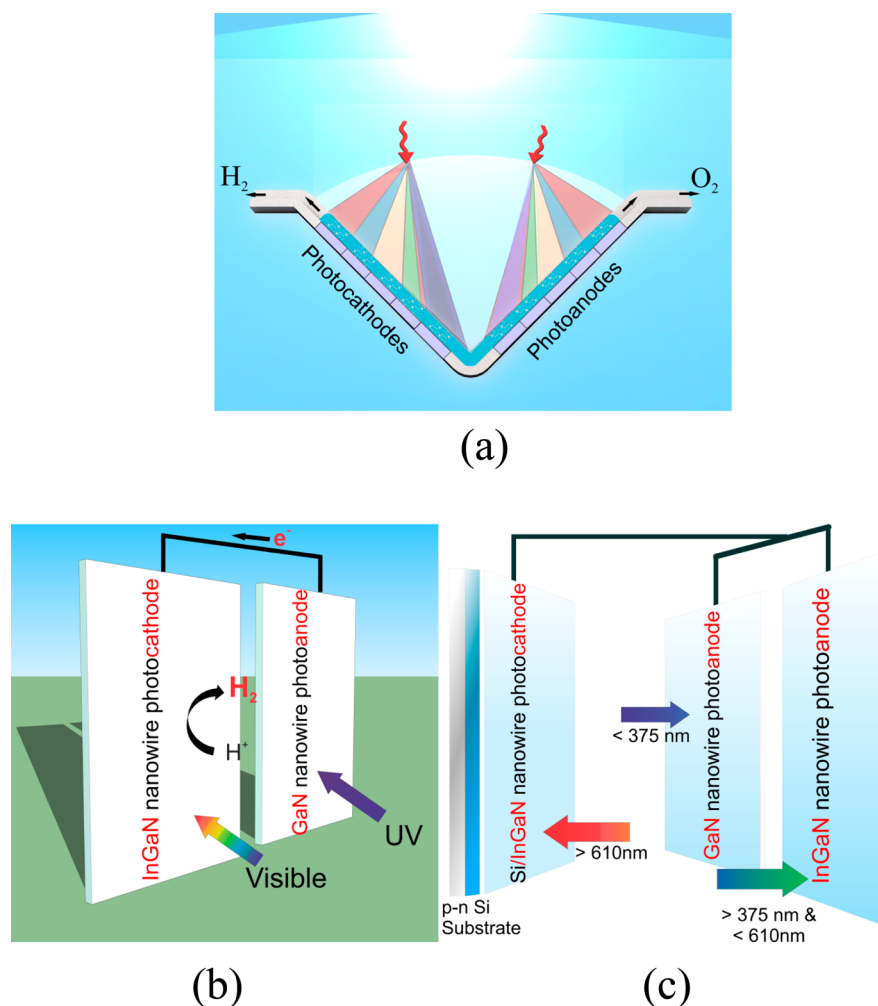
Figure 1. (a) Schematic illustration of the general concept of a dual-photoelectrode system under parallel illumination with the incident sunlight split spatially and spectrally on the photoanode and photocathode. Each photoanode (or photocathode) may consist of several parallel-connected anodes (or cathodes), each of which is illuminated with a portion of the solar spectrum in commensurate with its energy bandgap and light absorption capacity. While the current matching between the photoanode and photocathode is required, the current-matching for the parallel-connected photoanodes (or photocathodes) is not required, due to the parallel connection. (b) Schematic of the GaN nanowire photoanode and InGaN nanowire photocathode in a dual configuration, which are designed to absorb the UV and visible spectrum of sunlight, respectively. (c) Schematic of the GaN and InGaN nanowire photoanodes, which are connected in parallel and paired with the Si/InGaN photocathode. The incident sunlight is split spectrally and spatially among the photoelectrodes.

contact or tunnel junction connecting the electrodes. Also, due to the dissimilar material properties the optimum performance of the two electrodes may require the use of different electrolytes. For example, the previously reported n-WO$_3$/p-Si dual tandem photoelectrode only showed modestly enhanced photovoltage but with tremendous compromises in photocurrent and efficiency.[11,22,24−26]

In this context, we have developed for the first time metal-nitride nanowire-based dual-photoelectrode systems in acidic electrolyte (i.e., 1 mol/L HBr), which, together with the parallel illumination scheme, can fundamentally address these critical challenges. Metal-nitrides, for example, InGaN, can be doped n- or p-type and can support large current conduction. To date, it is the only material family whose energy band can be tuned across nearly the entire solar spectrum and whose band edges can uniquely straddle the H$^+$/H$_2$ and O$_2$/H$_2$O redox potentials under deep visible and near-infrared light irradiation.[27] Previously, the use of metal-nitrides as single photoelectrodes for solar-driven water splitting has been reported.[28−36] In this work, we have first demonstrated dual-photoelectrode devices

consisting of an n-GaN nanowire photoanode and a p-InGaN nanowire photocathode, which are directly grown on low cost, large area Si substrates. Under parallel illumination, the device exhibited an open circuit potential of 1.3 V and nearly 20-fold enhancement in the power conversion efficiency, compared to the individual photoelectrodes. We have further demonstrated a dual-photoelectrode system consisting of GaN/InGaN nanowire photoanodes and a Si/InGaN photocathode, which can perform unassisted, direct solar-to-hydrogen conversion. Under parallel light illumination by splitting the sunlight spatially and spectrally, a power conversion efficiency of 2% is achieved across the entire solar spectrum, which is more than 1 order of magnitude higher than the individual photoelectrodes.

Schematic of the side-by-side dual-photoelectrode design is illustrated in Figure 1a. The solar spectrum is split spatially and spectrally, and different light spectra are spread out to strike the corresponding single-band photoelectrodes. Compared to conventional tandem configuration, the unique parallel illumination scheme offers several distinct advantages. First, it provides a better degree of flexibility in optimizing the
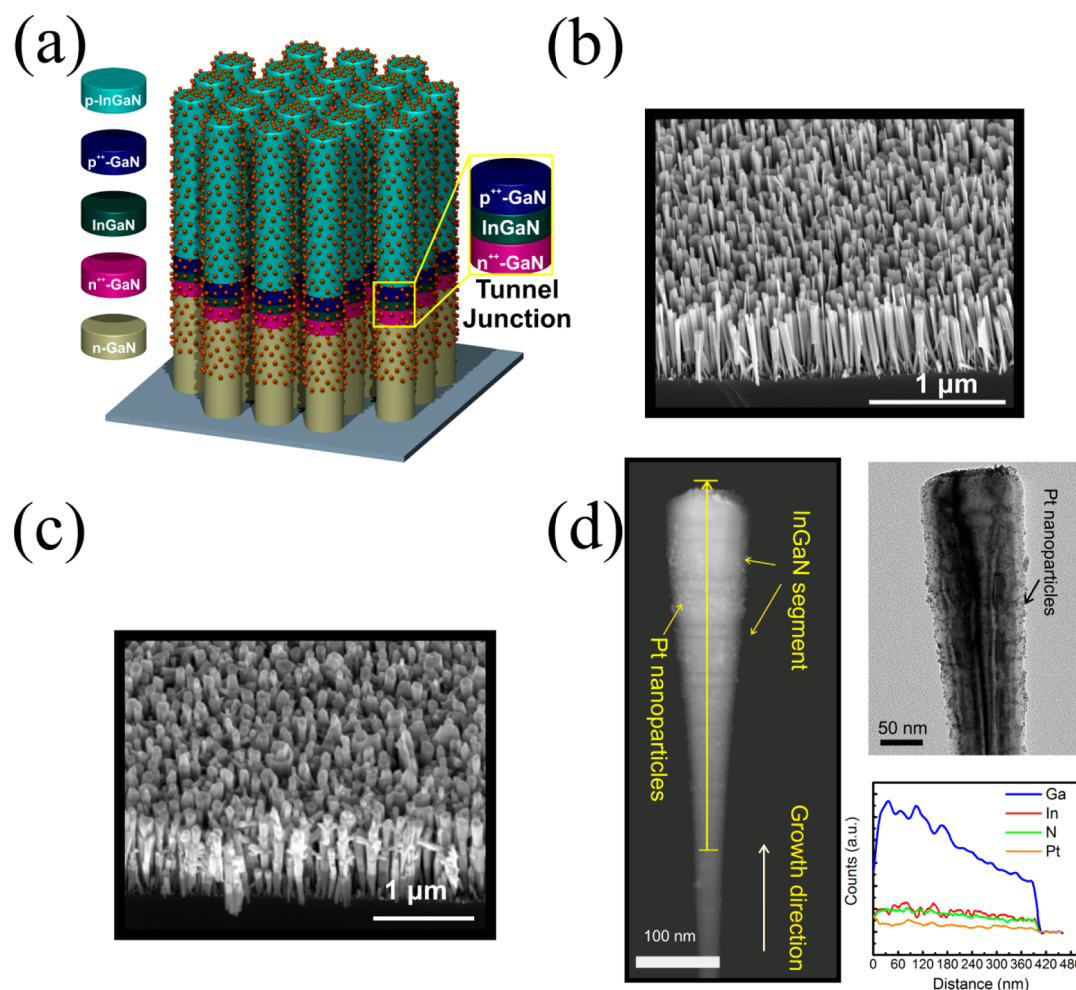
Figure 2. (a) Schematic of the p-InGaN nanowire photocathode connected directly with a low resistivity n-Si substrate through a polarization-enhanced tunnel junction. The presence of Pt nanoparticle cocatalyst is also shown. (b) A 45° tilted SEM image of as-grown GaN nanowires on n-Si substrate. (c) A 45° tilted SEM image of p-InGaN nanowires grown on n-Si substrate decorated with Pt nanoparticles. (d) STEM-HAADF image of a single p-InGaN nanowire (left). Variations of the In Lα, Ga Kα, and N Kα signals analyzed by EDXS along the nanowire axial direction (along the yellow arrow) is shown in the lower right. The uniform coverage of Pt nanoparticles on the nanowire lateral surfaces is shown in the upper right.

photovoltage and photocurrent of a dual-photoelectrode device by splitting the sunlight spectrally and spatially in commensurate with the energy bandgap and light absorption capacity of the photoanodes and photocathodes. Second, the concept of parallel illumination can be extended to the design of parallel-connected multiphotoanodes (or photocathodes) with complementary bandgap. As the multiphotoanodes (or multiphotocathodes) are connected in parallel, current matching is not required: the photocurrent generated by each photoanode (or photocathode) will add up to the total photocurrent of the photoanode (or photocathode). Moreover, the parallel-connected multiphotoanodes (or multiphotocathodes) possess an onset potential that can be as large as any of its single photoelectrode can provide. Such parallel-connected photoanodes (or photocathodes) can offer both large photovoltage and high photocurrent and can break the Shockley−Quaisser limit of a single bandgap photoanode (or photocathode). This concept resembles the current-unconstrained multijunction solar cells,[37,38] wherein the energy loss associated with carrier thermalization can be minimized, or eliminated. The power conversion efficiency of such devices can reach up to 64.9%.[38] Moreover, the surface area and light intensity of each electrode can be separately controlled,[8] providing additional dimensions

to optimize the current matching and open circuit potential and thereby leading to maximum efficiency.

To validate the design flexibility and efficiency enhancement, we have investigated two prototypes of devices consisting of In(Ga)N nanowire photocathodes and photoanodes with complementary bandgaps. The first design, schematically shown in Figure 1b, is comprised of a GaN nanowire photoanode and an InGaN nanowire photocathode, which are designed to absorb the UV and visible spectrum of sunlight, respectively. The second structure incorporates a parallel-connected GaN nanowire and InGaN nanowire photoanode and a Si/InGaN photocathode, illustrated in Figure 1c. The GaN nanowire photoanode, InGaN photoanode, and Si/InGaN photocathode are separately illuminated with wavelengths <375, 375−610, and >610 nm, respectively, by splitting the solar spectrum.

The design, fabrication, and performance of paired GaN nanowire photoanode and InGaN nanowire photocathode device is first described. In this experiment, catalyst-free InGaN and GaN nanowires were grown on n-type Si(111) substrate by radio frequency plasma-assisted molecular beam epitaxy (MBE) under nitrogen-rich conditions (Supporting Information S1). The InGaN nanowire photocathode consists of p-InGaN, a

polarization enhanced tunnel junction, n-GaN, and n-type Si substrate, shown in Figure 2a. With the use of tunnel junction, p-InGaN nanowire photocathodes can be monolithically integrated on a low resistivity n-Si substrate. Detailed analysis of the tunnel junction was described elsewhere.[39] Scanning electron microscopy (SEM) images of GaN and InGaN nanowires are shown in Figure 2b,c, respectively. The nanowires are vertically aligned on the Si substrate. The diameters are in the range of 40−100 nm, and the areal density is ∼5 × 10^9 cm^{-2}. Pt cocatalysts were formed on p-InGaN nanowire surfaces by using a photodeposition method (Supporting Information S2). In this process, Pt nanoparticles were preferentially reduced on the active sites of the nanowire surfaces by photogenerated electrons. The structural properties of p-InGaN were analyzed by scanning transmission electron microscopy (STEM). A HAADF image of a p-InGaN nanowire decorated by Pt nanoparticles is illustrated in Figure 2d. The nanowire length is ∼600 nm. The elemental distribution in the nanowire was analyzed by energy dispersive X-ray spectrometry (EDXS). Variations of the In Lα, Ga Kα, and N Kα signals along the nanowire axial direction (yellow line in (HAADF image)) is shown in Figure 2d (lower right). The diameters of Pt nanoparticles are ∼1 nm. The TEM image shows uniformly distributed Pt nanoparticles along the lateral surfaces of the nanowire (upper right of Figure 2d).

Prior to the PEC experiments, Ohmic contact on the backside of the Si substrate was formed by applying Ga−In eutectic, which was connected to a Cu wire using silver paint. The sample backside was then covered by insulating epoxy. PEC properties of the nanowire photoelectrodes were first investigated using a quartz reaction chamber with a three-electrode configuration, consisting of a double junction Ag/AgCl reference electrode, a nanowire working electrode, and a Pt counter electrode. A 300 W xenon lamp, together with various optical filters, was used as the light source. The illumination intensity was measured using a thermocouple detector (Newport, 818P-100-55). An Interface1000 electro-chemical station (Gamry, Germany) was used throughout this study, and the scan rate of the applied potential was 20 mV/s. The conversion from Ag/AgCl to reversible hydrogen electrode (RHE) is computed using $E_{(RHE)} = E_{Ag/AgCl} + 0.059 \times pH + E°_{Ag/AgCl}$ (where $E°_{Ag/AgCl} = 0.197$ V and pH value is close to zero). In this study, we have used HBr as the electrolyte, which can be equally useful compared to water splitting.[40−42] Moreover, the presented photoelectrode design and concept can be readily applied to other systems for H_2O reduction and oxidation.

A linear sweep voltammogram for the GaN nanowire photoanode was performed under both dark and illumination conditions, shown in Figure 3a. The onset potential of the photoanode is −0.3 V (versus RHE). Upon illumination, the measured current density is saturated at 45 mA/cm^2 at 0.25 V (versus RHE). The decrease of the photocurrent when saturated can be attributed to several factors, including the change of the local concentration around the electrodes of the redox species due to the high current produced, heating effect, and the bubbles of the produced gases. The average incident-photon-to-current efficiency (IPCE) in the UV range is ∼85%, which is higher than previously reported large bandgap materials.[43−46] E_{OCP} versus RHE of GaN under dark and illumination conditions is shown Figure 3b. Upon illumination, the E_{OCP} of GaN nanowire photoanode is ∼−0.3 V, which is consistent with the onset potential. The potential difference

(a)

(b)

(c)
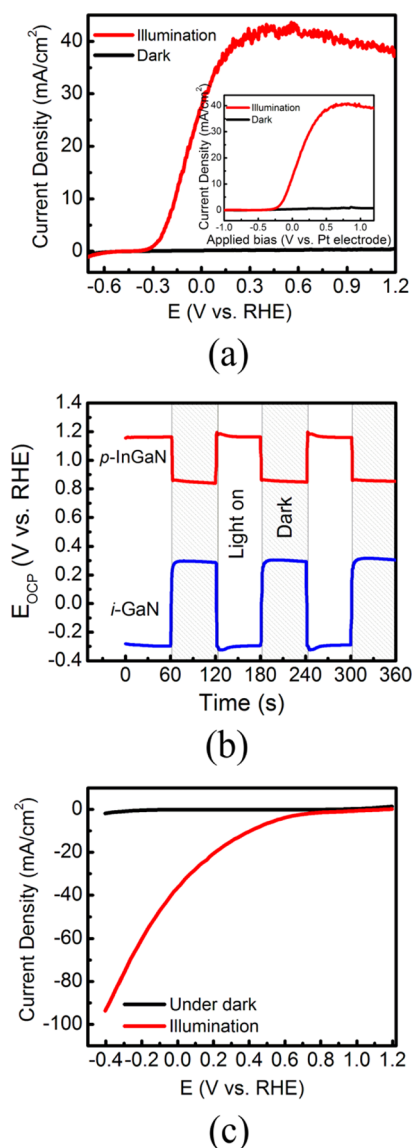
Figure 3. (a) $J−E$ curves of GaN nanowire photoanode under dark and illumination conditions. A 300 W xenon lamp was used as an outer irradiation source. The GaN photoanode onset potential occurred at −0.3 V (versus RHE). The inset shows $J−V$ versus Pt electrode in a two-electrode configuration. (b) Open-circuit potential E_{OCP} of the GaN nanowire photoanode and InGaN nanowire photocathode. The potential difference between illumination and dark conditions are ∼0.6 and 0.3 V for the GaN photoanode and InGaN photocathode, respectively. (c) $J−E$ curve of InGaN nanowire photocathode under dark and illumination conditions. The onset voltage of the InGaN photocathode occurs at ∼1 V (versus RHE).

under illumination and dark of the GaN photoanode is ∼0.6 V, which is close to the band bending V_{fb}.

The $J−E$ curve of p-InGaN nanowire photocathode was first measured using a full arc xenon lamp equipped with an AM1.5G filter, shown in Figure 3c. The onset potential is ∼1 V (versus RHE), and the current density increases to ∼95 mA/cm^2 at −0.4 V (versus RHE). The open-circuit potential difference under illumination and dark is ∼0.3 V, illustrated in Figure 3b, which shows the behavior of p-type semiconductor. It is worth noting that the E_{OCP} of the photocathode and photoanode extend beyond the redox potentials, which can minimize the need for external electric energy to achieve
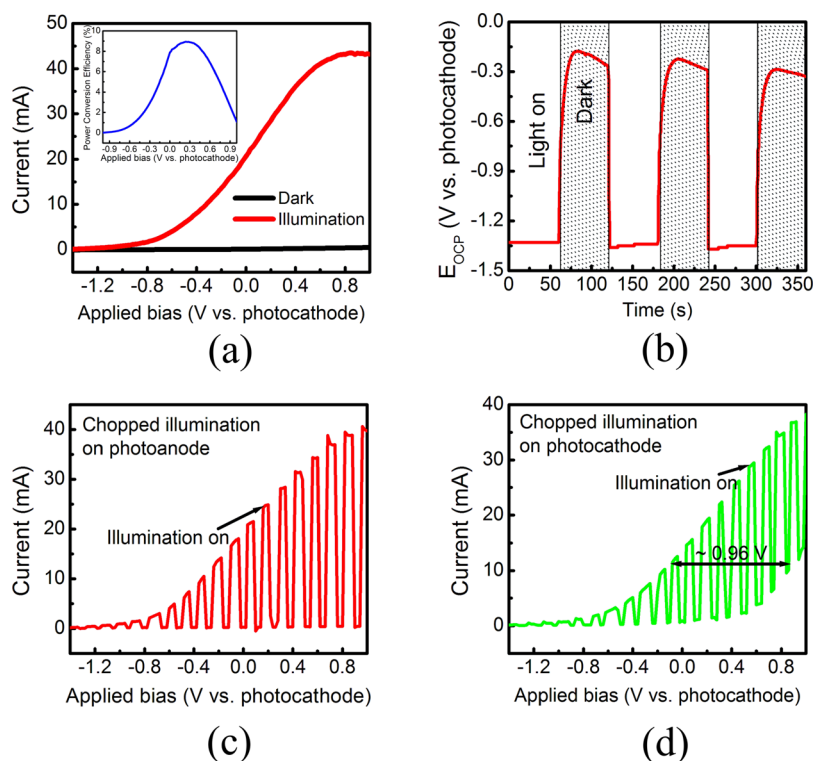
Figure 4. (a) $I-V$ curve of the paired GaN nanowire photoanode and InGaN nanowire photocathode under dark and illumination conditions. The photoanode and photocathode were illuminated with wavelengths of 300−400 and 400−600 nm and power densities of ∼120 and 160 mW/cm², respectively. The power conversion efficiency of the dual-photoelectrode device versus applied bias is shown in the inset. The maximum power conversion efficiency is ∼9%, which occurs at ∼0.3 V versus the photocathode. (b) Open-circuit potential (E_{OCP}) of the dual-photoelectrode. (c) $I-V$ curve of the dual-photoelectrode device with the photocathode and photoanode under continuous and chopped illumination, respectively. With no illumination on the photoanode, the current density approaches zero, due to the current matching requirement. (d) $I-V$ curve of the dual-photoelectrode with the photoanode under continuous illumination and the photocathode under chopped illumination. The measured photocurrent is nonzero even when there is no illumination on the photocathode, because the Pt-decorated nanowires on the photocathode can act as a catalyst for hydrogen evolution reaction.

maximum efficiency for the dual-photoelectrode device described below. The $J-V$ curve and E_{OCP} of the InGaN nanowire photocathode under visible light illumination (400−600 nm) was also studied and shown in Supporting Information S4. The IPCE at −0.4 V versus RHE is shown in Supporting Information S4. The maximum IPCE is ∼65% at 350 nm. The IPCE drops to 45% at the wavelength of 400 nm and further decreases toward longer wavelengths (>600 nm), which outperforms some previously reported photocathode materials.[47−52]

Subsequently, the n-GaN photoanode and p-InGaN photocathode were connected to form a dual-photoelectrode device, schematically shown in Figure 1b. The GaN photoanode and the InGaN photocathode were separately illuminated with wavelengths of 300−400 and 400−600 nm and power densities of ∼120 and 160 mW/cm², respectively. The sample areas of both photoelectrodes are ∼1 cm². A linear sweep voltammogram of the dual-photoelectrode is shown in Figure 4a. The short-circuit current of the dual-photoelectrode is ∼20 mA/cm², and the current density is saturated at ∼43 mA/cm² above 0.7 V (versus the photocathode). The onset potential occurred at −1.2 V (versus the photocathode), which is consistent with the open circuit measurement shown in Figure 4b. The nearly 1 V onset potential shift compared to the GaN photoanode versus Pt counter electrode (inset of Figure 3a) is due to the synergetic effect of the dual-photoelectrode. Shown in Figure 4b, the open circuit potential of the dual-photoelectrode is

∼−1.3 V versus the photocathode under illumination, which is interpreted as the difference of the Fermi levels of the photoanode and the photocathode. The open circuit potential is consistent with the onset potential shown in Figure 4a. Under dark conditions, the open circuit potential is −0.2 V versus the photocathode.

To further study the effect of the dual-photoelectrode, linear sweep voltammogram measurements were performed with the light source chopped on either the photoanode or the photocathode. Shown in Figure 4c, when the illumination on the photoanode was blocked, no photocurrent could be measured, which is limited by the current matching requirement. However, when the illumination on the photocathode was blocked, pronounced photocurrent could still be measured, shown in Figure 4d. The $I-V$ shows ∼1 V shift, compared to that when both photoelectrodes were illuminated. This interesting phenomena is explained by that photogenerated electrons from the photoanode can be injected into the photocathode and drive hydrogen evolution reaction (HER) through the Pt-decorated nanowire segment.[39] The power conversion efficiency of the dual-photoelectrode device was derived using the following equation

$$\eta(\%) = \frac{I(E_{rev}^0 - V_{app})}{P_{in}} \times 100 \tag{1}$$

where I is the photocurrent, E_{rev}^0 is the standard state-reversible potential (i.e., 1.07 V for Br$^-$), V_{app} is the actual applied bias between the working electrode and the counter electrode, and P_{in} is the power of the incident light. Variations of the power conversion efficiency versus applied bias is shown in the inset of Figure 4a. A maximum power conversion efficiency of ∼9% was measured at 0.3 V (versus the photocathode). For comparison, the power conversion efficiency of the stand-alone InGaN photocathode is only 0.5% under visible light illumination (400−600 nm). The nearly 20-fold enhancement in the power conversion efficiency clearly demonstrates the distinct advantages of a dual-photoelectrode device under parallel illumination.[53,54]

For practical applications, the bandgaps of the two photoelectrodes should be approximately 1.7 and 1.0 eV in order to optimize solar absorption. In this regard, we have investigated the second prototype device, consisting of GaN and InGaN nanowire photoanodes, which are connected in parallel, and a Si/InGaN nanowire photocathode, schematically shown in Figure 1b (Supporting Information S6 and S7). The bandgaps of InGaN nanowire photoanode and Si are ∼2.0 and 1.1 eV, respectively. The Si/InGaN nanowire photocathode consists of p-InGaN/tunnel junction/n-GaN nanowire arrays grown directly on a Si solar cell. Such a photocathode can effectively absorb near-infrared light irradiation and provide relatively high onset potential.[39] Schematic of the device is shown in Supporting Information S6 and was also reported previously.[39] PEC experiments were performed separately on the GaN nanowire photoanode, InGaN nanowire photoanode, and Si/InGaN photocathode under AM1.5G 1 sun illumination using an Oriel LCS-100 (Newport) solar simulator. The PV-InGaN-nanowire-cathode was decorated with Pt nanoparticles. Figure 5a shows $J−E$ characteristics of the GaN and InGaN nanowire photoanodes whose onset potentials are −0.3 and 0.6 V (versus RHE), respectively. The saturation current of the GaN nanowire photoanode is ∼1 mA/cm^2, whereas the photocurrent density of the InGaN-nanowire-anode reaches ∼4.7 mA/cm^2 at 1.2 V (versus RHE). This current density of the InGaN nanowire photoanode corresponds to an average IPCE of ∼40% in the wavelength range of 300−610 nm. The $J−E$ curve of the InGaN nanowire photoanode under 375−610 nm illumination is also shown in Figure 5a, which confirms most of the photocurrent is due to the visible light illumination. The onset potential of the photocathode is ∼0.5 V (versus RHE) while the saturation current is ∼19 mA/cm^2 (Supporting Information S6) under AM1.5G 1 sun illumination. The onset potential remained the same and the saturation photocurrent was reduced to ∼14 mA/cm^2 under >610 nm illumination.

The GaN and InGaN nanowire photoanodes were subsequently paired with the Si/InGaN photocathode, schematically shown in Figure 1c. The sample areas of the GaN and InGaN nanowire photoanodes and Si/InGaN nanowire photocathode are 1, 1, and 0.45 cm^2, which were illuminated with light in the wavelength ranges of <375, 375−610, and >610 nm, respectively. The combination of these illuminations resembles the full spectrum of AM1.5G. Shown in Figure 5b, the $I−V$ curve follows that of the parallel-connected GaN and InGaN nanowire photoanodes, due to the current matching requirement. The onset potential is −0.6 V versus the photocathode. At zero bias (0 V versus the photocathode), the photocurrent of the device is ∼0.9 mA, which leads to a power conversion efficiency of 1.5%. The applied bias photon-to-current efficiency (ABPE) is further calculated using eq 1 and is

(a)

(b)

(c)
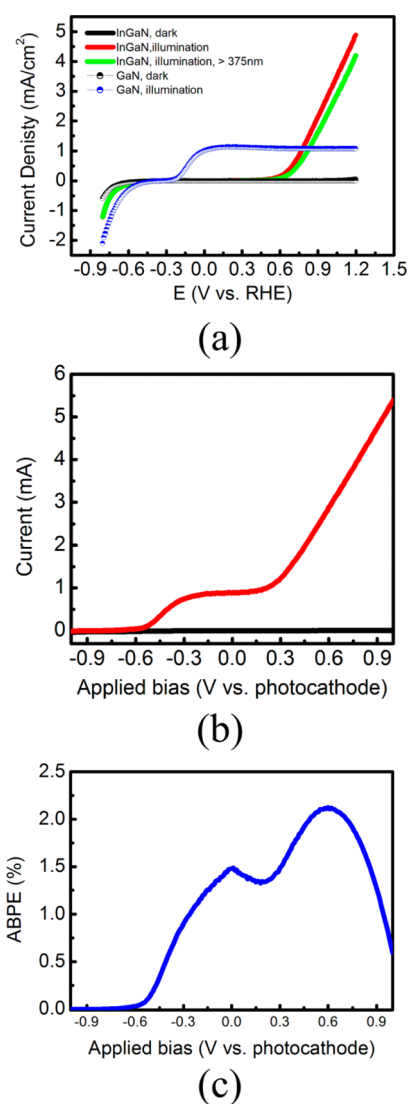
Figure 5. (a) $J−E$ curves of the GaN and InGaN nanowire photoanodes under dark and illumination conditions. An AM1.5G 1 sun solar simulator was used as the outer irradiation source. Also shown in the figure is the $J−E$ curve of the InGaN nanowire photoanode under visible light illumination (375−610 nm) (green curve). (b) $I−V$ curve of the dual-photoelectrode consisting of a GaN and InGaN nanowire photoanode and a Si/InGaN nanowire photocathode under dark and AM1.5G 1 sun illumination conditions. The sunlight was spectrally and spatially split on the three electrodes. The GaN nanowire photoanode, InGaN nanowire photoanode, and Si/InGaN nanowire photocathode were illuminated with light in the wavelength ranges of <375, 375−610, and >610 nm, respectively. (c) The power conversion efficiency of the dual-photoelectrode device as a function of applied bias under AM1.5G 1 sun illumination. The maximum power conversion efficiency is ∼2%, which occurs at ∼0.6 V versus the photocathode.

plotted in Figure 5c. A maximum ABPE of ∼2% was measured at ∼0.6 V versus the photocathode, which is nearly 14-fold higher than the ABPE (∼0.15%) of the stand-alone InGaN nanowire photoanode under simulated sunlight illumination (Supporting Information S7). The efficiency can be further improved by increasing the photocurrent of the photoanode with enhanced indium incorporation and by optimizing the onset potentials of the photoanodes and photocathodes.

In conclusion, we have shown that the dual-photoelectrode device, in conjunction with the parallel illumination scheme and the extreme flexibility in bandgap engineering of metal-nitride nanowire structures, can enhance the power conversion efficiency by more than 1 order of magnitude, compared to that of the individual photoelectrodes. In this configuration, the large bandgap photoelectrode provides high open circuit potential, while photocurrent matching can be readily achieved by splitting the solar spectrum in commensurate with bandgap engineering. Moreover, both the photovoltage and photocurrent can be optimized by connecting multiphotoanodes (or photocathodes) in parallel. The significantly enhanced power conversion efficiency is unprecedented for a dual-photoelectrode device and clearly illustrates the extraordinary potential of metal-nitride nanowire photoelectrodes, in conjunction with the parallel illumination scheme, for achieving high efficiency, unassisted solar-to-hydrogen conversion.

■ ASSOCIATED CONTENT

ⓈSupporting Information

The Supporting Information is available free of charge on the ACS Publications website at DOI: 10.1021/acs.nanolett.5b02671.

> MBE growth, photodeposition of Pt co-catalyst, PEC characterization measurements, PEC properties of InGaN nanowire photocathode, structural characterization, fabrication and characterization Si/InGaN nanowire photocathode, characterization of InGaN nanowire photoanode, additional figures, and additional references. (PDF)

■ AUTHOR INFORMATION

Corresponding Author

*E-mail: zetian.mi@mcgill.ca. Phone: 1 514 398 7114.

Notes

The authors declare no competing financial interest.

■ ACKNOWLEDGMENTS

■ REFERENCES

(1) Ciamician, G. *Science* **1912**, *36*, 385−394.

(2) Walter, M. G.; Warren, E. L.; McKone, J. R.; Boettcher, S. W.; Mi, Q. X.; Santori, E. A.; Lewis, N. S. *Chem. Rev.* **2010**, *110*, 6446−6473.

(3) Tachibana, Y.; Vayssieres, L.; Durrant, J. R. *Nat. Photonics* **2012**, *6*, 511−518.

(4) Li, Y.; Zhang, J. Z. *Laser Photonics Rev.* **2010**, *4*, 517−528.

(5) Bolts, J. M.; Ellis, A. B.; Legg, K. D.; Wrighton, M. S. *J. Am. Chem. Soc.* **1977**, *99*, 4826−4827.

(6) Fornarini, L.; Nozik, A. J.; Parkinson, B. A. *J. Phys. Chem.* **1984**, *88*, 3238−3243.

(7) LaTempa, T. J.; Rani, S.; Bao, N. Z.; Grimes, C. A. *Nanoscale* **2012**, *4*, 2245−2250.

(8) Ding, C. M.; Qin, W.; Wang, N.; Liu, G. J.; Wang, Z. L.; Yan, P. L.; Shi, J. Y.; Li, C. *Phys. Chem. Chem. Phys.* **2014**, *16*, 15608−15614.

(9) Seger, B.; Castelli, I. E.; Vesborg, P. C. K.; Jacobsen, K. W.; Hansen, O.; Chorkendorff, I. *Energy Environ. Sci.* **2014**, *7*, 2397−2413.

(10) Hu, S.; Xiang, C. X.; Haussener, S.; Berger, A. D.; Lewis, N. S. *Energy Environ. Sci.* **2013**, *6*, 2984−2993.

(11) Coridan, R. H.; Shaner, M.; Wiggenhorn, C.; Brunschwig, B. S.; Lewis, N. S. *J. Phys. Chem. C* **2013**, *117*, 6949−6957.

(12) Jang, J.-W.; Du, C.; Ye, Y.; Lin, Y.; Yao, X.; Thorne, J.; Liu, E.; McMahon, G.; Zhu, J.; Javey, A.; Guo, J.; Wang, D. *Nat. Commun.* **2015**, *6*, 7447.

(13) Nozik, A. J. *Appl. Phys. Lett.* **1977**, *30*, 567−569.

(14) Yoneyama, H.; Sakamoto, H.; Tamura, H. *Electrochim. Acta* **1975**, *20*, 341−345.

(15) Kim, T. W.; Choi, K. S. *Science* **2014**, *343*, 990−994.

(16) Rai, S.; Ikram, A.; Sahai, S.; Dass, S.; Shrivastav, R.; Satsangi, V. R. *RSC Adv.* **2014**, *4*, 17671−17679.

(17) Hanna, M. C.; Nozik, A. J. *J. Appl. Phys.* **2006**, *100*, 074510.

(18) Khaselev, O.; Bansal, A.; Turner, J. A. *Int. J. Hydrogen Energy* **2001**, *26*, 127−132.

(19) Miller, E. L.; Rocheleau, R. E.; Khan, S. *Int. J. Hydrogen Energy* **2004**, *29*, 907−914.

(20) Han, L. H.; Digdaya, I. A.; Buijs, T. W. F.; Abdi, F. F.; Huang, Z. Q.; Liu, R.; Dam, B.; Zeman, M.; Smith, W. A.; Smets, A. H. M. *J. Mater. Chem. A* **2015**, *3*, 4155−4162.

(21) Han, L. H.; Abdi, F. F.; Rodriguez, P. P.; Dam, B.; van de Krol, R.; Zeman, M.; Smets, A. H. M. *Phys. Chem. Chem. Phys.* **2014**, *16*, 4220−4229.

(22) Coridan, R. H.; Arpin, K. A.; Brunschwig, B. S.; Braun, P. V.; Lewis, N. S. *Nano Lett.* **2014**, *14*, 2310−2317.

(23) Khaselev, O.; Turner, J. A. *Science* **1998**, *280*, 425−427.

(24) Yoon, K. H.; Shin, C. W.; Kang, D. H. *J. Appl. Phys.* **1997**, *81*, 7024−7029.

(25) Yoon, K. H.; Seo, D. K.; Cho, Y. S.; Kang, D. H. *J. Appl. Phys.* **1998**, *84*, 3954−3959.

(26) Singh, T.; Muller, R.; Singh, J.; Mathur, S. *Appl. Surf. Sci.* **2015**, *347*, 448−453.

(27) Moses, P. G.; Van de Walle, C. G. *Appl. Phys. Lett.* **2010**, *96*, 021908.

(28) Fujii, K.; Ohkawa, K. *Jpn. J. Appl. Phys. 2* **2005**, *44*, L909−L911.

(29) Fujii, K.; Nakamura, S.; Yokojima, S.; Goto, T.; Yao, T.; Sugiyama, M.; Nakano, Y. *J. Phys. Chem. C* **2011**, *115*, 25165−25169.

(30) AlOtaibi, B.; Nguyen, H. P. T.; Zhao, S.; Kibria, M. G.; Fan, S.; Mi, Z. *Nano Lett.* **2013**, *13*, 4356−4361.

(31) AlOtaibi, B.; Harati, M.; Fan, S.; Zhao, S.; Nguyen, H. P. T.; Kibria, M. G.; Mi, Z. *Nanotechnology* **2013**, *24*, 175401.

(32) Kibria, M. G.; Zhao, S.; Chowdhury, F. A.; Wang, Q.; Nguyen, H. P. T.; Trudeau, M. L.; Guo, H.; Mi, Z. *Nat. Commun.* **2014**, *5*, 3825.

(33) Ebaid, M.; Kang, J.-H.; Lim, S.-H.; Cho, Y.-H.; Ryu, S.-W. *RSC Adv.* **2015**, *5*, 23303−23310.

(34) Ebaid, M.; Kang, J.-H.; Ryu, S.-W. *J. Electrochem. Soc.* **2015**, *162*, H264−H270.

(35) Juodkazytė, J.; Šebeka, B.; Savickaja, I.; Kadys, A.; Jelmakas, E.; Grinys, T.; Juodkazis, S.; Juodkazis, K.; Malinauskas, T. *Sol. Energy Mater. Sol. Cells* **2014**, *130*, 36−41.

(36) Akimov, A. V.; Muckerman, J. T.; Prezhdo, O. V. *J. Am. Chem. Soc.* **2013**, *135*, 8682−8691.

(37) Brown, A. S.; Green, M. A. *Phys. E* **2002**, *14*, 96−100.

(38) Brown, A. S.; Green, M. A. *Prog. Photovoltaics* **2002**, *10*, 299−307.

(39) Fan, S.; AlOtaibi, B.; Woo, S. Y.; Wang, Y.; Botton, G. A.; Mi, Z. *Nano Lett.* **2015**, *15*, 2721−2726.

(40) Bard, A. J.; Fox, M. A. *Acc. Chem. Res.* **1995**, *28*, 141−145.

(41) White, J. R.; Fan, F. R. F.; Bard, A. J. *J. Electrochem. Soc.* **1985**, *132*, 544−550.

(42) Johnson, E. L.; Kilby, J. S. *Fourth E.C. Photovoltaic Solar Energy Conference*; Bloss, W. H., Grassi, G., Eds.; Springer: Netherlands, 1982; pp 611−615.

(43) Pan, Z.; Qiu, Y.; Yang, J.; Liu, M.; Zhou, L.; Xu, Y.; Sheng, L.; Zhao, X.; Zhang, Y. *J. Mater. Chem. A* **2015**, *3*, 4004−4009.

(44) Gurudayal; Chee, P. M.; Boix, P. P.; Ge, H.; Yanan, F.; Barber, J.; Wong, L. H. *ACS Appl. Mater. Interfaces* **2015**, *7*, 6852−6859.

(45) Ren, W.; Zhang, H.; Kong, D.; Liu, B.; Yang, Y.; Cheng, C. *Phys. Chem. Chem. Phys.* **2014**, *16*, 22953−22957.

(46) Chen, W.; Qiu, Y.; Yang, S. *Phys. Chem. Chem. Phys.* **2012**, *14*, 10872−10881.

(47) Iwase, A.; Ng, Y. H.; Amal, R.; Kudo, A. *J. Mater. Chem. A* **2015**, *3*, 8566−8570.

(48) Liu, J.; Hisatomi, T.; Ma, G.; Iwanaga, A.; Minegishi, T.; Moriya, Y.; Katayama, M.; Kubota, J.; Domen, K. *Energy Environ. Sci.* **2014**, *7*, 2239−2242.

(49) Nakabayashi, Y.; Nishikawa, M.; Nosaka, Y. *Electrochim. Acta* **2014**, *125*, 191−198.

(50) Sharma, D.; Verma, A.; Satsangi, V. R.; Shrivastav, R.; Dass, S. *Int. J. Hydrogen Energy* **2014**, *39*, 4189−4197.

(51) Hu, Y.; Dong, W.; Zheng, F.; Fang, L.; Shen, M. *Appl. Phys. Lett.* **2014**, *105*, 082903.

(52) Guan, Z.; Luo, W.; Zou, Z. *CrystEngComm* **2014**, *16*, 2929−2936.

(53) Dahal, R.; Pantha, B. N.; Li, J.; Lin, J. Y.; Jiang, H. X. *Appl. Phys. Lett.* **2014**, *104*, 143901.

(54) Alvi, N. H.; Rodriguez, P. E. D. S.; Kumar, P.; Gomez, V. J.; Aseev, P.; Alvi, A. H.; Alvi, M. A.; Willander, M.; Notzel, R. *Appl. Phys. Lett.* **2014**, *104*, 223104.